Skeletal Muscle NAD(P)H Two-Photon Fluorescence Microscopy In Vivo: Topology and Optical Inner Filters

Emily C. Rothstein, Stefanie Carroll, Christian A. Combs, Paul D. Jobsis, and Robert S. Balaban
Laboratory of Cardiac Energetics, National Heart, Lung and Blood Institute, National Institutes of Health, Department of Human Health Services, Bethesda, Maryland

ABSTRACT Two-photon excitation fluorescence microscopy (TPEFM) permits the investigation of the topology of intercellular events within living animals. TPEFM was used to monitor the distribution of mitochondrial reduced nicotinamide adenine dinucleotide (NAD(P)H) in murine skeletal muscle in vivo. NAD(P)H fluorescence emission was monitored (~460 nm) using 710–720 nm excitation. High-resolution TPEFM images were collected up to a depth of 150 μm from the surface of the tibialis anterior muscle. The NAD(P)H fluorescence images revealed subcellular structures consistent with subsarcolemmal, perivascular, intersarcomeric, and paranuclear mitochondria. In vivo fiber typing between IIB and IIA/D fibers was possible using the distribution and content of mitochondria from the NAD(P)H fluorescence signal. The intersarcomeric mitochondria concentrated at the Z-line in the IIB fiber types resulting in a periodic pattern with a spacing of one sarcomere (2.34 $\pm$ 0.17 μm). The primary inner filter effects were nearly equivalent to water, however, the secondary inner filter effects were highly significant and dynamically affected the observed emission frequency and amplitude of the NAD(P)H fluorescence signal. These data demonstrate the feasibility, and highlight the complexity, of using NAD(P)H TPEFM in skeletal muscle to characterize the topology and metabolic function of mitochondria within the living mouse.

INTRODUCTION

Two-photon excitation fluorescence microscopy (TPEFM) (Denk et al., 1990) permits the monitoring of subcellular events in thick samples (Denk et al., 1994; Kasischke et al., 2004; Zipfel et al., 2003) as well as living animals (for review see Cahalan et al., 2002). Using this approach, many investigators have been able to monitor processes under in vivo conditions, which previously could be examined only in isolated cells (Chen et al., 2000; Dunn et al., 2002; Helmchen et al., 1999; Kleinfeld et al., 1998; Larson et al., 2003; Levene et al., 2004; Masters et al., 1997; Squirrell et al., 1999; Svoboda et al., 1997). In this study, we explored the use of TPEFM to evaluate murine skeletal muscle morphology and energetics using reduced nicotinamide adenine dinucleotide (NAD(P)H) fluorescence. NAD(P)H has been previously shown to have an adequate two-photon cross-sectional area for TPEFM studies (Huang et al., 2002; Kierdaszuk et al., 1996). We hypothesized that the NAD(P)H signal would be primarily from mitochondria and would thus provide an intrinsic marker of their distribution as well as provide specific information on their redox state.

Mitochondria are organized in skeletal muscle in patterns that may facilitate metabolic or signaling functions. Extensive characterization of skeletal muscle structure has been performed over the years and mitochondrial distribution in fixed tissue samples is well understood (Hamalainen and Pette, 1993; Hoppeler et al., 1973; Leeson and Leeson, 1969; Stenger et al., 1962). There are four major pools of mitochondria in skeletal muscle: subsarcolemmal, perivascular, intersarcomeric, and paranuclear. The plasticity of skeletal muscle mitochondria content is evident in the adaptation to alterations in activity levels and environmental factors such as microgravity, hypoxia, and strength training (Hoppeler and Fluck, 2003). For example, endurance training (Hoppeler et al., 1973), unlike strength training (Chilibeck et al., 1999), has been shown to increase the volume of intersarcomeric mitochondria. Although different functions and characteristics have been ascribed to these different pools of mitochondria, via differential isolation techniques (for review see Hoppeler and Fluck, 2003), the role of these different compartments of mitochondria is still poorly defined. In addition to the intercellular distribution of mitochondria, their overall concentration generally decreases along the fiber type continuum from slow to fast (i.e., Type I, IIA, IID/X, IIB). Previous ultrastructural studies of human tissue have shown that slow twitch Type I fibers have more intersarcomeric mitochondria that align more along the Z-line as the fibers tend toward fast twitch Type IIB fibers (Ogata and Yamasaki, 1997). This distribution is consistent with the more aerobic activity of Type I fibers. In the mouse, skeletal muscle contains predominantly the fast muscle Types IIA, IID, and IIB (Hamalainen and Pette, 1993; Sartorius et al., 1998). For the purposes of this study, we have grossly classified the fiber types commonly seen in mouse skeletal muscle into Type IIB and Type IIA/D fibers, with fiber Type IIB containing less mitochondria, as previously confirmed using NADH tetraxolium reductase activity (Hamalainen and Pette, 1993). The differential distribution

Submitted September 20, 2004, and accepted for publication November 18, 2004.

Address reprint requests to Dr. Emily C. Rothstein, LCE, NHLBI, National Institutes of Health, Bldg. 10, Rm. B1D416, 9000 Rockville Pike, Bethesda, MD 20892. E-mail: emilyr@nih.gov.

© 2005 by the Biophysical Society

0006-3495/05/03/2165/12 $2.00

doi: 10.1529/biophysj.104.053165

of mitochondria in these fiber types suggests that mitochondrial NAD(P)H fluorescence could be used to assign skeletal muscle fiber type noninvasively in vivo.

When excited in the ultraviolet (UV), tissue NAD(P)H emits a blue fluorescence in the 440 nm region (Chance and Baltscheffsky, 1958) that is influenced by its microenvironment (Avi-Dor et al., 1963; Blinova et al., 2004; Chance et al., 1962; Estabrook, 1962). As originally demonstrated by Chance and colleagues, endogenous NAD(P)H fluorescence is a useful marker for mitochondrial distribution in cells as well as a redox marker of their metabolic state (Chance et al., 1962). In many tissues it has been demonstrated that the mitochondrial NAD(P)H pool dominates the emission signal due to its high concentration and enhanced lifetime (Chance et al., 1962; Eng et al., 1989; Koretsky et al., 1987; Nuutinen, 1984). However, the nature of the NAD(P)H emission signal in murine skeletal muscle has not been well defined in vivo. TPEFM has the distinct advantage of monitoring NAD(P)H deep in tissues because infrared light is used for excitation rather than ultraviolet light (Piston et al., 1995). This minimizes, but does not eliminate, the scattering and primary inner filter effects on the excitation light, but the secondary filter effects on the emitted light can be significant microns deep into the tissue (Brandes et al., 1994; Chance et al., 1962; Fralix et al., 1990; Koretsky et al., 1987). Thus, to interpret TPEFM, care must be taken to compensate for signal changes resulting from secondary filtering by the tissue.

The purpose of this study was to image the distribution of NAD(P)H in intact murine muscles using TPEFM. The distribution of the NAD(P)H signal was evaluated as to whether it was consistent with a mitochondrial origin, whether the different intracellular pools of mitochondria were distinguishable and whether the NAD(P)H signal can be used for fiber typing in vivo. Finally, the ability to qualitatively follow the NAD(P)H redox state using TPEFM through the primary and secondary inner filters of the skeletal muscle was assessed using spectrafluorometric approaches.

MATERIALS AND METHODS

Light and electron microscopy histology

The mouse (CD-1) tibialis anterior (TA) was fixed with 2.5% glutaraldehyde in 0.1 M phosphate buffer (pH 7.4) for 1 h and was then postfixed with 1% osmium tetroxide in phosphate buffer for 1 h at 4°C. After dehydration with graded ethanol, the tissue was embedded in EMbed 812. One-micron sections were cut and stained with toluidene blue and analyzed with a light microscope. Ultrathin sections were then cut, stained with 3% uranyl acetate and 2% lead citrate, and examined in a transmission electron microscope (EM) (JEOL 1200 EX) (JEOL USA, Peabody, MA).

In vivo mouse preparation

For initial induction of anesthesia, each mouse (CD-1 strain) was placed in a mouse anesthesia box (VetEquip, Pleasanton, CA) aired with 2.5% isoflurane and 30% oxygen. Once anesthetized, the mouse was removed from the box and anesthesia was administered as 2.5% isoflurane and 30% oxygen through a nose cone to the mouse. The TA was exposed by first removing the fur with shaving and treatment with the depilatory Nair. The skin and fascia were resected to expose the TA. A custom-designed mouse leg restraint was used, which held the muscle in constant tension to minimize motion and bathed it in a saline solution to permit the use of the 20× water immersion objective. The mouse was placed under the microscope with an internal temperature monitoring control using a specialized heating board (Indus Instruments, Houston, TX), modified to fit on the microscope stage.

TPEFM

In vivo, NAD(P)H TPEFM imaging was performed using a Bio-Rad Radiance-2100 multiphoton instrument (Bio-Rad Laboratories, Hercules, CA) with an ''upright'' Nikon E600FN microscope and a Spectra-Physics Tsunami laser (Spectra-Physics, Mountain View, CA) tuned to emit 720 nm light with ~10 mW power at the back aperture of the objective. A 20×/0.95W XLUMPlanFl Olympus water immersion objective was used. NAD(P)H TPEFM imaging was also monitored on an inverted Zeiss LSM510 microscope (Carl Zeiss, Thornwood, NY) with excitation by a Coherent Chameleon laser at 710–720 nm with a c-Achroplan 40×/0.80W Zeiss objective. Intrinsic NAD(P)H fluorescence was generally monitored at 380–550 nm. Specific acquisition parameters are provided in the figure legends.

TPEFM spectroscopic imaging

TPEFM emission spectroscopy was conducted on ex vivo tissue on an inverted Zeiss LSM510 with the META microscope spectroscopy attachment. Excitation was accomplished with a Coherent Chameleon laser at 710–720 nm with 10 mW power at back aperture of a 20×/0.75 air Zeiss objective. Using 720 nm excitation, the spectral characteristics of fluorescence emission ranging from 382- to 628-nm wavelengths on the mouse TA ex vivo were monitored using a Zeiss LSM510 META system. Fluorescence emission was collected in 5 μm slices from skeletal muscle beginning at the location where skeletal muscle fibers were first clearly imaged to 70 μm into the tissue.

Data were analyzed using custom-designed software written in IDL (RSI, Boulder, CO) and KaleidaGraph 3.5 (Synergy Software, Reading, PA). The spectral sensitivity calibration of the Zeiss META System was performed as previously reported (Jöbsis et al., 2004).

Estimated sarcomere length from fluorescence images

Mitochondrial NAD(P)H fluorescence was used to estimate sarcomere length in vivo relying on the dominate deposition of mitochondria at the Z-line. The average sarcomere length was determined within individual cells of the mouse TA using a Fourier transform (FFT) analysis of the NAD(P)H signal intensity as a function of distance using custom-designed software written in IDL (RSI). Regions of interest were selected from the original image files containing a sarcomere field. For filtering purposes, a Hanning window was applied to reduce edge effects and a minimum (1–2 μm) and maximum (5–6 μm) spacing size, converted to spatial frequency, was used to mask the FFT data. Data are presented as a power spectrum of the filtered FFT data versus spacing distance.

Enzymatic dissociation of mouse skeletal muscle and confocal microscopy analysis

The enzymatic dissociation method has been modified from a protocol previously described (Carroll et al., 1995). The extensor digitorum longus (EDL) and soleus muscle were dissected from mice immediately after sacrifice and were pinned by the tendons to a Sylgard-lined dissecting dish.

The muscles were incubated at 37°C for 3–4 h in Ringer's solution ((in mM) 2.7 KCl, 1.2 KH_2PO_4, 0.5 $MgCl_2$, 138 NaCl, 8.1 $NaHPO_4$, 1.0 $CaCl_2$; pH 7.4) containing 0.2% Type I collagenase (Sigma, St. Louis, MO). After incubation, muscles were washed twice with Ringer's solution and triturated to completely dissociate the muscles into individual intact fibers. Dissociated fibers were plated onto laminin-coated glass-bottom culture dishes. NAD(P)H fluorescence was observed with a Zeiss 510 LSM confocal microscope and a 63×/0.90 water immersion objective (Carl Zeiss, Thornwood, NY). NAD(P)H fluorescence images of these fibers were obtained using 351 nm excitation and a 430 nm high-pass filter for emission detection.

Single-photon emission spectroscopy

On the same preparations used in the in vivo TPEFM studies, but without the saline bath, single-photon emission and absorption high-resolution spectroscopy were performed to better characterize the extent and consequences of tissue secondary filter properties in the visible light region. Fluorescence emission studies were conducted using a bifurcated fiber optic (Ocean Optics, Dunedin, FL) with one port used to impinge 360 nm light (from a Hg-Xe 500 W light source) on the exposed muscle while the other port was used to collect the emitted light and direct it to a rapid scanning spectrophotometer resident in a personal computer (Ocean Optics). This system permitted high spectral (~1 nm) and temporal (<100 ms) resolution spectroscopy data to be collected from essentially the same preparations used in the TPEFM studies.

Data were analyzed using custom-designed software written in IDL (RSI). The difference spectrum was achieved by subtraction of a reference spectrum (data point R) from selected data spectrum at each selected time during the experiment.

Near infrared tissue absorbance

The primary absorbance of near infrared (NIR) light was determined for several organs from mice using freshly homogenized tissue. The homogenized tissues were used to prevent sieving of light through heterogeneous tissues and to permit the homogeneous distribution of reference compounds for estimation of photon pathlengths in the tissue (Wilson et al., 1989). Data were collected within an integrating sphere (Bose et al., 2003; Latimer and Rabinowitch, 1959) to minimize scattering effects on absorption but required the determination of pathlength for comparison between different tissues and different wavelengths. Heart, liver, kidney, brain, and hind-leg skeletal muscle (primarily fast-twitch glycolytic) tissues were collected from 15 mice (CD-1) in three batches of five mice each. With each mouse under isofluorane (2.5%) anesthesia, the vena cava was partially cut and the right ventricle was catheterized using a 22-gauge needle to perfuse the entire animal with saline. The saline perfusion was used to reduce the influence of hemoglobin on tissue spectra. Once the tissue and circulatory effluent appeared to be cleared of blood, the tissues were removed and cleaned of fat and fascia. One gram of tissue was placed in 2 ml 0.1 mM sodium phosphate buffer (pH 7.0) and homogenized using mechanical and glass homogenizers at ~4°C. Samples were usually deoxygenated by normal tissue respiration even at ~4°C. In some tissues, full oxygenation was achieved by five minutes of bubbling with 100% oxygen and then rapidly sampling the tissue. In more metabolically active tissues, heart and liver, 10 μl rotenone (7.8 mM) and 10 μl antimycin A (150 mM) were added to block oxygen consumption but to keep cytochrome *c* oxidase oxidized and myoglobin oxygenated. Because NAD(P)H, FAD and cytochromes *c* and *b* have minimal NIR absorbances, reduction of these chromophores by this inhibition scheme was assumed to be insignificant in the NIR spectrum.

NIR to visible spectra of 3 ml tissue homogenates were measured using a Lambda 800 dual beam spectrophotometer (Perkin Elmer, Wellesley, MA) equipped with a 150-mm center mount integrating sphere. The integrating sphere with a center-mounted sample allowed the collection of most of the scattered light from these highly scattering samples. However, the relative photon pathlength in different tissues or different wavelengths in the same tissue needed to be determined. To accomplish this task, a known absorbance standard, 5 μl of 1:80 v/v dilution of India ink (Standford, Bellwood, IL) in buffer was added to the sample after this initial absorption measurement and the specimen was rescanned to estimate the scattered pathlength in the sample. The additional absorbance of the ink in the scattering solution was compared to its absorbance in buffer alone. The ratio of the scattering to nonscattering absorbance was used as an estimate of the pathlength, and was used as a correction factor to calculate the true sample absorbance assuming that the small absorbance of the India ink did not significantly affect the pathlength through the sample. In addition, spiking of tissue samples with known amounts of a reference compound Alexafluor 750 (Molecular Probes, Eugene, OR) in scattering medium was used to test the validity of this approach. Using this spiking approach as an estimate of measurement errors, we found that a consistent 10% over estimate of true absorbance was apparent in the region of NIR absorbance measured from the tissues. This systematic error is likely due to imperfections in the integrating sphere collection scheme. This correction as a function of wavelength was made in all calculated tissue absorbances reported.

RESULTS

Histology

To aid in the interpretation of the fluorescence data, we undertook light and EM histology of the murine TA with special attention to the distribution of mitochondria. Because we are only monitoring mitochondrial content and distribution in this study, we are limiting our fiber type characterization to Type IIA/D (higher mitochondrial content) and Type IIB (lower mitochondrial content) fibers consistent with previous histological characterization (Brooke and Kaiser, 1970). At low power light microscopy using toluidene blue stain (see Fig. 1 *A*), more mitochondria were present in a subset of smaller fibers, which is consistent with a slower fiber type (Brooke and Kaiser, 1970). Also apparent at this magnification was the large concentration of mitochondria in intersarcomeric and perivascular regions.

A representative EM image of a Type IIB fiber is shown in Fig. 1 *C*, which reveals a periodic pattern resulting from a preferential location of mitochondria on either side of the t-tubule at the Z-line. In the Type IIA/D fibers, the distribution was located in a similar pattern but with mitochondria spanning several sarcomeres that resulted in strips of mitochondria running along the long axis of the myocyte. A representative EM image from a perivascular zone is presented in Fig. 1 *B*. The mitochondria are found lining the vascular space with some regions having mitochondrial clusters of 3–6 deep. These perivascular clusters of mitochondria were most prevalent in the Type IIA/D fibers.

Isolated muscle fibers

The correlation between the UV-excited blue fluorescence in mouse skeletal muscle and the mitochondrial distribution was evaluated using enzymatically assisted isolation of fast-twitch EDL muscles (88% Type IIB) (Raymackers et al.,

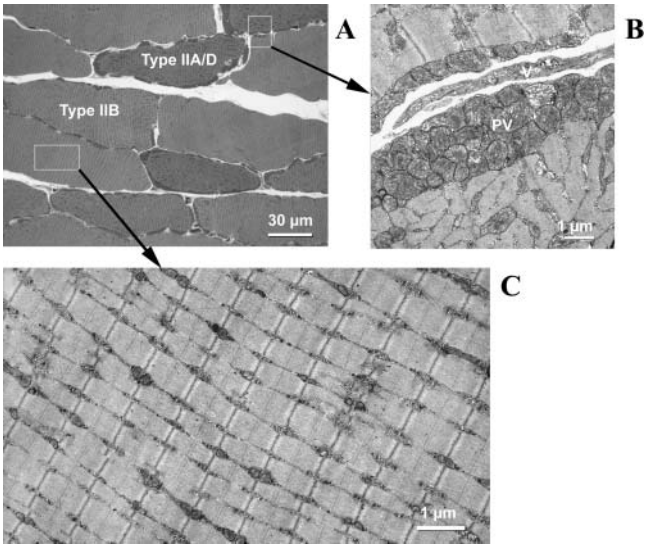

FIGURE 1 Mouse TA topology. (*A*) Light microscopy (1 μm section) of the mouse TA. Muscle fiber morphology is consistent with conventional mouse skeletal fiber types of Type IIB and Type IIA/D (Hamalainen and Pette, 1993; Sartorius et al., 1998). (*B*) EM of the mouse TA shows the perivascular mitochondrial (*PV*) pattern in the skeletal muscle around vessels (*V*). (*C*) EM in Type IIB reveals the deposition of mitochondria at the intersection of fibers along the Z-line. Scale bars shown represent 30 μm in panel *A*, and 1 μm in panels *B* and *C*.

2000) or slower-twitch soleus muscles (~65% Type IIA/D) (Totsuka et al., 2003). Representative fluorescence images from these fibers are presented in Fig. 2. The Type IIB fibers had less blue fluorescence emission (~450 nm) intensity (47% less than Type IIA/D) and demonstrated a striking Z-line localization of the fluorescence (Fig. 2 *A*), which is consistent with the distribution of mitochondria observed in the histology studies. In Type IIA/D fibers (Fig. 2 *B*), the Z-line distribution of mitochondria was less prevalent with many streaks of fluorescence running along several sarcomeres. This distribution of fluorescence is similar to the

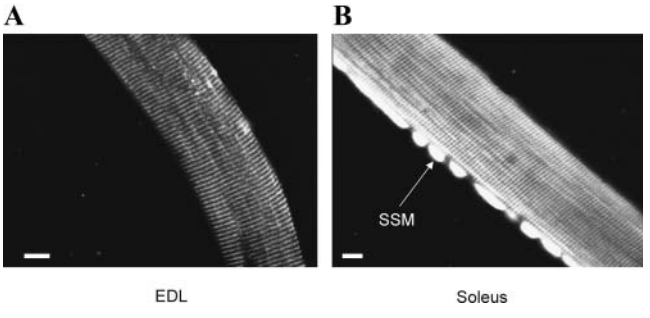

FIGURE 2 NAD(P)H fluorescence images of isolated mouse skeletal muscle fibers. Single fibers isolated from the mouse (*A*) EDL muscle and (*B*) soleus muscle imaged for NAD(P)H fluorescence. Subsarcolemmal mitochondria (*SSM*) were evident in the isolated soleus muscle, which is consistent with the in vivo observations. The SSM in these isolated fibers could also represent the perivascular mitochondrial pool. Scale bars shown in both panels *A* and *B* represent 10 μm.

mitochondrial distribution in Type IIA/D fibers along the length of sarcomeres, as observed in the histology studies. In addition, subsarcolemmal clusters of fluorescence were observed in the Type IIA/D fibers that might represent residual perivascular mitochondrial clusters in the isolated fibers. To confirm the mitochondrial source of the fluorescence, cyanide was added to both types of cells. Cyanide increased the fluorescence emission (~300%) from both types of cells without altering the distribution patterns, which is consistent with the notion that this signal is dominated by mitochondrial NAD(P)H. The same distributions of NAD(P)H fluorescence in these fiber types were observed using TPEFM (710–720 nm excitation) suggesting that the cross-sectional areas are still dominated by the mitochondrial NAD(P)H.

These studies support the notion that the UV-excited blue fluorescence from murine skeletal muscle is dominated by mitochondrial NAD(P)H fluorescence, and that this intrinsic mitochondrial NAD(P)H signal can be used to assess the fiber type (i.e., Type IIB or Type IIA/D) based on the distribution of mitochondria. Based on these results, we assume that the blue fluorescence signal from murine muscle fibers in TPEFM originates from mitochondrial NAD(P)H.

TPEFM in vivo

In our initial studies, tissue motion was a significant problem even with a framing rate of 1 s. This was not surprising because we were attempting to collect data in the order of 1 μm resolution in breathing, living animal. The biggest source of motion was due to respiratory activity. Using the constant tension scheme outlined above we were able to hold the upper leg far enough away from the body to reduce respiratory motion artifacts without interfering with blood perfusion as judged by laser Doppler flow (not shown).

Once a stable specimen was obtained, we found that we could generate high-quality blue fluorescence images to a depth of 150 μm with ~25–75 mW of laser power at the back focal plane. The in-plane resolution was >2 μm since the Z-lines of the muscle could be resolved (see below). The higher power levels, which are necessary for imaging deeper into the muscle, elicited direct morphological changes that suggested some type of photodynamic damage if used to image near the surface of the tissue. However, when imaging at tissue depths beyond ~80 μm, we did not observe these morphological changes with high power levels, suggesting that the NIR-induced damage is indeed both power and depth dependent in tissue in vivo. A montage of samples from a series of images taken in the Z-plane (up to 150 μm into the tissue, with the first image of myocytes as the starting point at 0 μm) is presented in Fig. 3, and an individual image at 150 μm is presented in Fig. 4 *B*. From these images, it is clear that individual cells, nuclei (dark circular structures), vascular spaces (dark cylindrical structures), and intracellular structures (Z-lines) can be distinguished using the blue

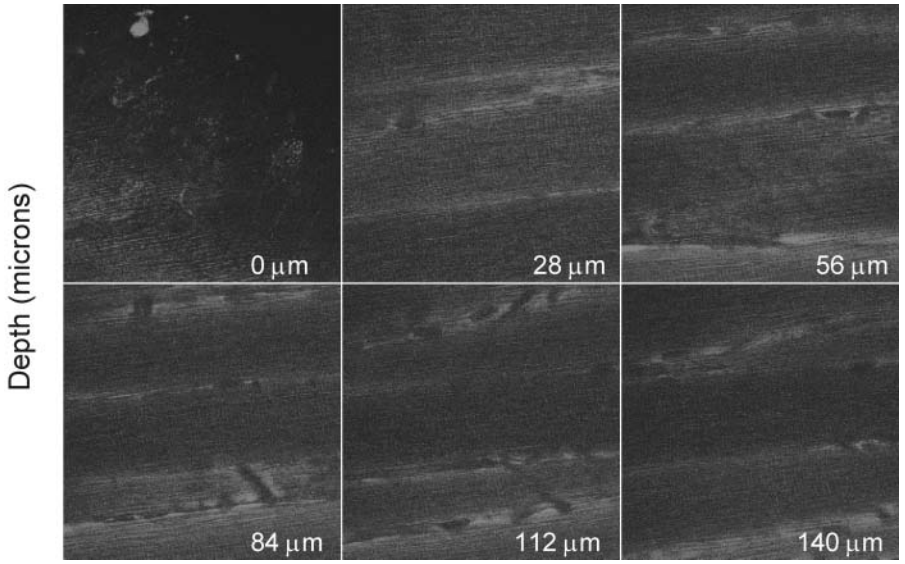

FIGURE 3 Montage of a z-stack of NAD(P)H fluorescence images from a mouse TA in vivo. NAD(P)H fluorescence was imaged in 1 μm optical sections from the first site where myocytes were visible (0 μm location) to 150 μm deep into the TA. Every 28th image is presented beginning with 11 μm into the stack at the top left-hand corner and with depth running in a left-to-right direction. The depths of the images are given as a reference; 0.636 μm pixel size, 10.464 μs dwell time, 720 nm excitation, 8-bit resolution, and 410–490 nm emission monitored.

fluorescence signal. The patterns of the blue florescence signal were consistent with a mitochondrial origin because they tracked the distribution of mitochondria found in the histology and fluorescence studies of single fibers. At the cellular level, brighter or darker fluorescent cells could be routinely identified that are consistent with IIA/D and IIB fiber types with a fluorescence distribution similar to that found in isolated muscle fibers (Fig. 2). On the intracellular level, subsarcolemmal, perivascular, paranuclear, and intersarcomeric clusters of fluorescence were routinely observed, which are consistent with the subsarcolemmal, perivascular, paranuclear, and intersarcomeric populations of mitochondria (Fig. 4 *B*). The Type IIA/D fibers exhibited a predominantly streaked blue fluorescence pattern consistent with an intersarcomeric distribution of NAD(P)H. Within the Type IIB muscle fibers, primarily a periodic fluorescence distribution was observed (see Fig. 4 *A*) that was consistent with the presence of mitochondria primarily located at the sarcomere junctions. To further analyze the periodic fluorescence in muscle fibers, the spacing between the signals was determined by performing a FFT of the fluorescence amplitude data along the long axes of the cells. Using this approach, the average fluorescence signal spacing was 2.34 ± 0.17 μm ($n = 6$) consistent with a Z-line spacing (see Fig. 5) and the mitochondria in the sarcomere junctions dominating the cellular fluorescence emission. Resolving these 2.3 μm structures suggests that the in-plane resolution is being maintained on the micron scale at this depth in the tissue.

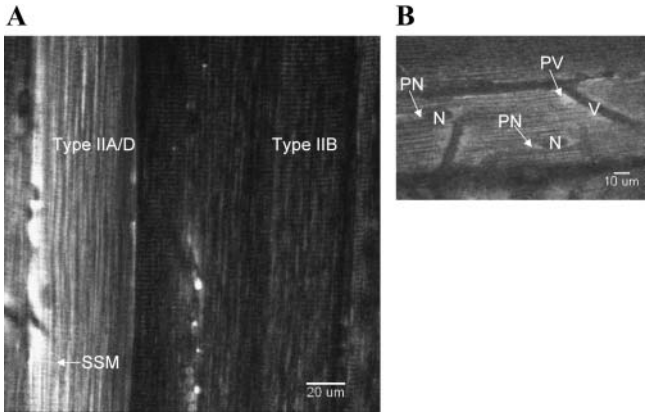

FIGURE 4 Illustrative NAD(P)H TPEFM images in mouse TA in vivo. (*A*) Illustration of Type IIB (*dark* highly striated) and Type IIA/D (*bright* fiber; long axis streaking of mitochondria and SSM pools) within the same field of view; 0.636-μm pixel size, 5.208-μs dwell time, 720-nm excitation, 8-bit resolution, and 410–490 nm emission monitored. (*B*) Vasculature (*V*) in the mouse TA is seen as voids in NAD(P)H fluorescence. Mitochondria are visualized through the NAD(P)H signal consistent with paranuclear (*PN*) and perivascular (*PV*) mitochondria. N represents nuclei; 0.190-μm pixel size, 1.60 μs dwell time, 720 nm excitation, 8-bit resolution, and 435–485 nm emission monitored. Scale bar shown in panel *A* represents 20 μm and in panel *B* represents 10 μm.

These morphological data are consistent with the notion that the blue fluorescence from mouse TA in vivo, is primarily from mitochondrial NAD(P)H and could be used for fiber typing using this intrinsic probe. In addition, the distribution of these signals in Type IIB fibers and in some Type IIA/D fibers may be used to estimate sarcomere spacing relatively noninvasively in vivo.

NIR tissue absorbance

An example of an NIR absorbance spectrum for the murine skeletal muscle homogenates and water is shown in Fig. 6. The absorbance of the skeletal muscle homogenate in the NIR only slightly exceeded the absorbance in pure water and the spectral characteristics did not change with oxygen tension (Fig. 6 *A*). Thus, for mouse skeletal muscle, the NIR

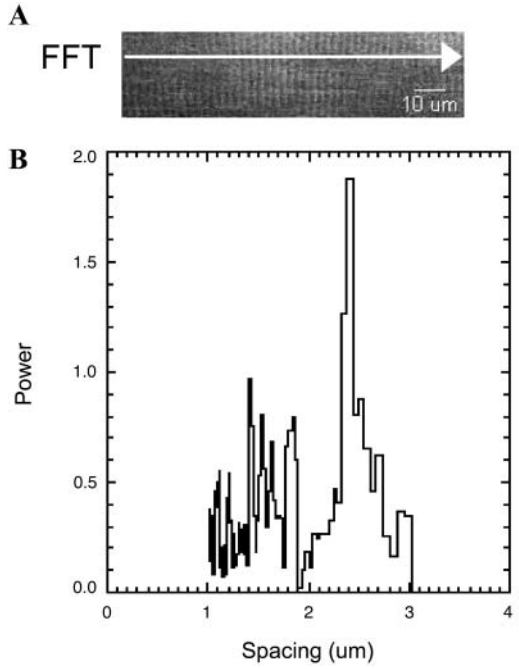

FIGURE 5 NAD(P)H fluorescence can be used to estimate sarcomere length in vivo. (*A*) FFT analysis is performed along the long axis of the cell in a NAD(P)H fluorescence image of a Type IIB fiber (image acquired with 720-nm excitation and 380–550 nm emission monitored with a 0.502 μm pixel size). (*B*) Filtered power spectrum of the long axis FFT. The average sarcomere length was 2.34 $\pm$ 0.17 μm ($n = 6$ fibers). Scale bar shown in panel *A* represents 10 μm.

absorbance is not a significant factor above the background water absorbance. However, this was not the case for all tissues studied, and the NIR absorbances for all tissues examined are summarized in Table 1. The spectral characteristics of the absorbances are consistent with a combination of cytochromes, myoglobin, and water, as shown in the heart tissue spectrum in Fig. 6 *B*. The high NIR absorbance in tissues such as heart and liver suggests that the primary tissue filter may be significantly above the water background. The oxygen dependence of the absorbance in heart (Table 1; Fig. 6 *B*) confirms the contribution of oxygen-sensitive tissue chromophores such as myoglobin and cytochromes, and also suggests that the primary filter could change depending on tissue oxygenation.

Secondary inner filter effects

In initial studies, we found that occlusion of the artery feeding the TA resulted in a transient decrease in NAD(P)H fluorescence when observing >50 μm within the muscle with TPEFM. This is the opposite from what is expected as the oxygen becomes rate limiting for oxidative phosphorylation and mitochondrial [NADH] increases, as previously seen in skeletal muscle (Chance and Schoener, 1962; Richmond et al., 1999). We reasoned that this was due to changes in secondary inner filters (from myoglobin, hemoglobin, and the cytochromes) on the emission signal during the early stages of ischemia. As previously demonstrated, secondary inner filters can significantly affect the NAD(P)H emission characteristics (Chance et al., 1962; Koretsky et al., 1987). It has been previously demonstrated that heart tissue causes a red shift in the NAD(P)H emission spectrum due to the preferential absorbance of 410–440 nm light by myoglobin and cytochromes (Koretsky et al., 1987).

We first attempted to measure the secondary inner filter effect in mouse muscle in vivo, using a simple one-photon UV excitation scheme (360 nm excitation) that grossly underestimated the secondary filter effects because the excitation penetrated much less than the 100 μm (Fralix et al., 1990) possible in TPEFM (Centonze and White, 1998), but permitted a detailed spectral analysis. This study was conducted by impinging the UV light on the resected muscle and collecting emission spectra before, during, and after a total arterial occlusion. For reference to the TPEFM experiment, the entire spectral bandwidth, theoretically, collected by the filter arrangement in TPEFM was analyzed by summing the emission spectrum from 380 to 560 nm. The time course of this emitted light from the leg is shown in Fig. 7 *A*. As observed in preliminary TPEFM experiments, the emission intensity initially dropped then increased during the occlusion followed by a large decrease in emitted light after

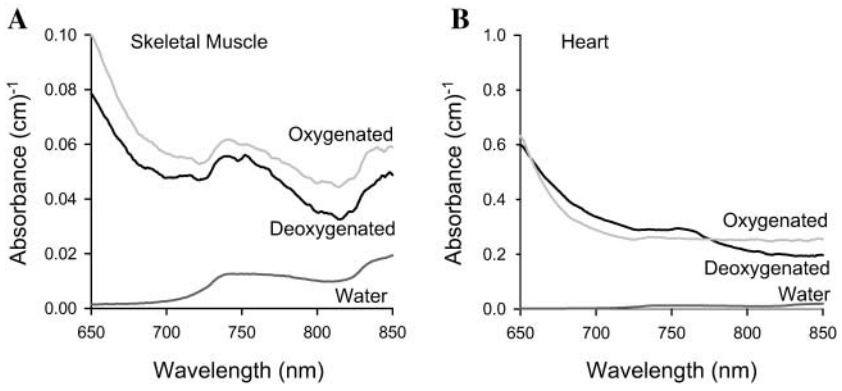

FIGURE 6 Near infrared absorbance spectra of water and mouse skeletal and heart muscle from 650 to 850 nm. (*A*) Near infrared absorbance (cm^{-1}) was determined for mouse skeletal muscle without hemoglobin. There is no substantial difference between oxygenated (*gray*) and deoxygenated (*black*) states, but both do appear to be influenced by the absorbance spectrum of water. However, the absorbance spectra (*B*) of oxygenated and deoxygenated heart tissue are insignificantly affected by water, but show substantial differences between oxygenated (*gray*) and deoxygenated (*black*) states. The degree of NIR absorbance of heart tissue may act as significant primary filter during TPEFM, whereas skeletal muscle NIR absorbance would only have a small primary filter effect similar to that of water.

TABLE 1 The primary absorbance of NIR light was determined for mouse tissues at 700, 750, 800, and 850 nm

	Oxygenated tissue absorbances (cm^{-1} of light path) ±SD			
	700 nm	750 nm	800 nm	850 nm
Heart	0.290 ± 0.045	0.259 ± 0.025	0.256 ± 0.014	0.263 ± 0.007
Liver	0.347 ± 0.074	0.243 ± 0.052	0.183 ± 0.044	0.160 ± 0.043
Kidney	0.232 ± 0.052	0.187 ± 0.043	0.162 ± 0.049	0.154 ± 0.051
Brain	0.053 ± 0.008	0.056 ± 0.010	0.043 ± 0.009	0.057 ± 0.010
Skeletal muscle	0.057 ± 0.010	0.060 ± 0.008	0.046 ± 0.008	0.060 ± 0.007
	Deoxygenated tissue absorbances (cm^{-1} of light path) ± SD			
	700 nm	750 nm	800 nm	850 nm
Heart	0.337 ± 0.014	0.290 ± 0.012	0.213 ± 0.025	0.197 ± 0.022
Liver	0.309 ± 0.070	0.226 ± 0.043	0.159 ± 0.031	0.141 ± 0.029
Kidney	0.277 ± 0.044	0.214 ± 0.032	0.149 ± 0.030	0.136 ± 0.031
Brain	0.045 ± 0.006	0.050 ± 0.007	0.033 ± 0.008	0.049 ± 0.012
Skeletal muscle	0.048 ± 0.005	0.055 ± 0.007	0.035 ± 0.005	0.049 ± 0.010

the reperfusion. To illustrate the spectral nature of these changes, individual spectra are presented in Fig. 8 *B* at different times as marked in Fig. 7 *A*. Even under control conditions, the tissue NAD(P)H emission (Fig. 7 *B*, spectrum *A*) was red-shifted relative to the emission frequency of bound mitochondrial NAD(P)H (~440 nm) (Blinova et al., 2004; Chance and Baltscheffsky, 1958) suggesting a secondary inner filter effect. The absolute spectra reflected the changes seen in the time course summed data. Difference spectroscopy was performed to highlight the spectral changes associated with these amplitude modifications. This was accomplished by taking the difference of all the spectra versus a reference point marked R. The resulting difference spectra for all of the sample spectra are presented in Fig. 7 *C*. With the onset of ischemia, the first spectral change was a large increase in apparent absorbance at ~436 nm along with smaller increases in the 500–550 nm wavelength range. These initial changes in the emission spectrum with ischemia are consistent with oxygenation changes in myoglobin or hemoglobin that precede any significant change in [NAD(P)H] due to the lower affinity of myoglobin/hemoglobin for oxygen when compared to the cytochrome chain (Tamura et al., 1978). Once the myoglobin/hemoglobin deoxygenation had been completed, as indicated by a stable 435 nm absorbance (see time course in Fig. 7 *D*), a large increase in the fluorescence signal at ~462 nm was observed that is spectrally consistent with an increase in NAD(P)H as oxygen becomes limiting for the cytochrome chain oxidation of NAD(P)H. Upon reflow, the absorbance from deoxymyoglobin rapidly disappears as oxygen is reintroduced. However, the 462 nm NAD(P)H signal dramatically decreases (see Fig. 7 *D*), which is consistent with the postischemia activation of metabolism (i.e., disrupted ion gradients, high Pi, ADP, creatine, etc.) or the so-called ''oxygen debt''. The temporal relationships of 435 and 462 nm emission are presented in Fig. 7 *D*. These data demonstrate that simply collecting bandwidth emission data in TPEFM in vivo can result in significant artifacts and difficulty in interpretation due to differential secondary inner filters.

To confirm the secondary inner filter effect in the TPEFM of muscle, the spectral properties of NAD(P)H emission were evaluated as a function of the image plane depth. The rationale of these studies was that the secondary filter effect should increase with the depth of penetration as the pathlength of the emitted light through the tissue increases. This was evaluated by taking advantage of the red shift induced in the NAD(P)H signal by the tissue secondary inner filter. Using a Zeiss META system with spectral corrections, we observed the red shift in fluorescence emission as a function of depth, from 0 (marked by the first image of myocytes) to 70 μm into tissues (Fig. 8), which is consistent with the secondary inner filter effect. These data are consistent with a significant influence of tissue secondary inner filters in TPEFM studies of NAD(P)H in skeletal muscle.

DISCUSSION

These studies demonstrate that TPEFM of NAD(P)H is feasible in mouse skeletal muscle, in vivo. These findings build on previous observations in other tissues and preparations (Huang et al., 2002; Kasischke et al., 2004; Konig et al., 1996; Piston et al., 1995). The morphological distribution and the cyanide sensitivity of NAD(P)H fluorescence are consistent with a dominant contribution from mitochondrial NAD(P)H as in other tissues (Chance and Thorell, 1959; Eng et al., 1989; Nuutinen, 1984). The different fiber types in the muscle could be delineated as well as several compartments of mitochondria, including the perivascular, paranuclear, and intersarcomeric populations using NAD(P)H TPEFM. The secondary inner filter effects and motion of the tissue were found to be very significant and required corrections to allow interpretation of amplitude

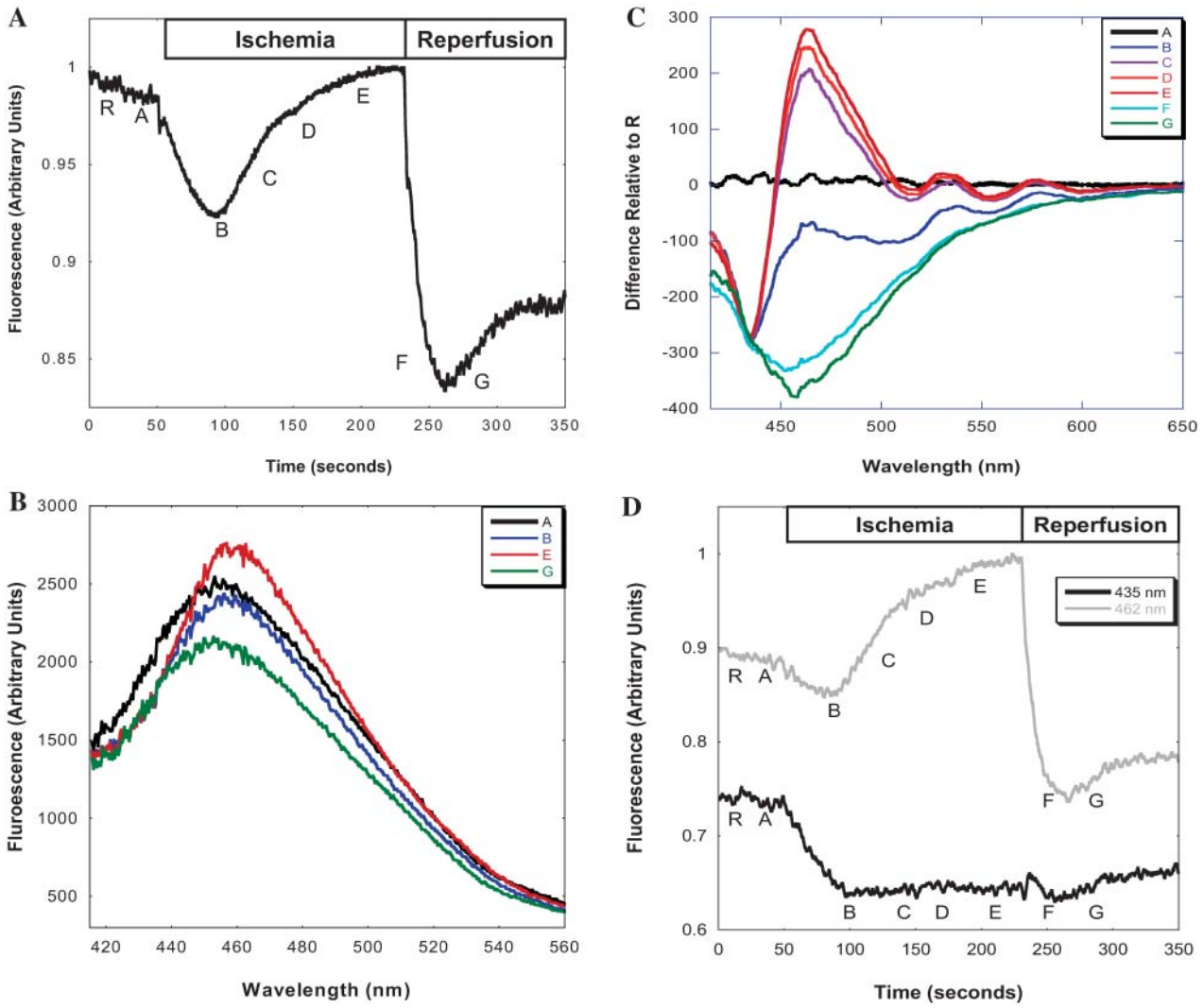

FIGURE 7 Effect of ischemia/reperfusion on NAD(P)H emission intensity from mouse TA in vivo. (*A*) Time course of normalized total emission intensity from 380 to 560 nm. The ischemia and reperfusion periods are indicated. Labeled experimental time points are listed as R (reference), A (control), B (early ischemia), C and D (mid-ischemia), E (late ischemia), F (early reperfusion), and G (reperfusion) for indexes to spectral data. (*B*) Fluorescence spectra from selected time points. (*C*) Difference spectra performed by subtracting the reference spectrum (R) from the index spectrum. (*D*) Fluorescence emission time courses (435 and 462 nm) illustrating the different temporal behavior of these two emission wavelengths through the protocol.

changes in NAD(P)H emission for correlation with mitochondrial metabolism.

The optical inner filters in skeletal muscle

Both primary and secondary filters are concerns in tissue microscopy studies. Using NIR excitation light, many of the primary filter effects associated with NAD(P)H excitation by UV light are minimized. In mouse skeletal muscle, the primary inner filter absorbance of 700–800 nm light was not much higher than water and did not change significantly with tissue oxygen (Fig. 6 *A*). However, in other tissues containing large amounts of myoglobin and mitochondria, such as heart, many more significant primary filters were observed that were altered by tissue oxygenation levels through the oxygen-sensitive chromophore absorbance (Fig. 6 *B*).

Primary filter effects may also play more of a role when the NIR passes through a large blood vessel in tissue in vivo where the absorbance by hemoglobin alone may be problematical. Thus, primary filters could influence the amplitude of the NAD(P)H emission as well as lead to photodynamic effects using the intense NIR illumination.

Another primary filter effect not extensively evaluated is the primary filter of the NIR light in the focal plane where the two-photon absorbance occurs. Others have shown that the absorbance of NIR light significantly increases at the focal plane (only 2–4 μm) when the photon density is sufficient to be absorbed by high concentrations of two-photon cross

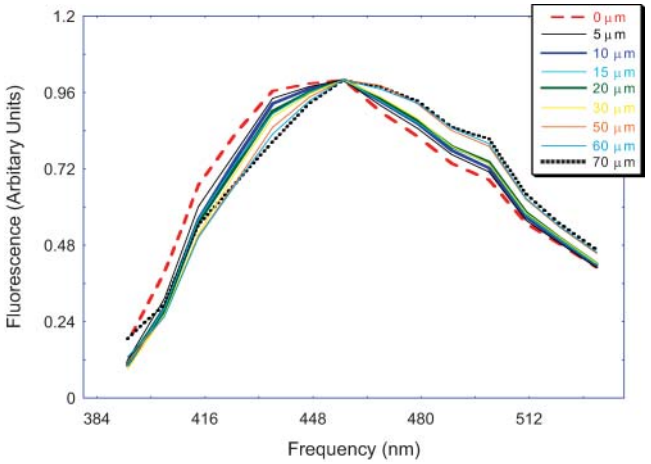

FIGURE 8 Secondary inner filter effects on NAD(P)H fluorescence in tissue. Two-photon NAD(P)H fluorescence was monitored with increasing tissue depth from the first site where myocytes were visible (0 μm location) up to 80 μm deep into the tissue using 720 nm excitation. NAD(P)H fluorescence (382–628 nm) using the Zeiss META in lambda mode. Data were normalized and showed peak fluorescence near 460 nm.

sections in the sample (Sheik-Bahae et al., 1990). Because the total number of UV-absorbing molecules in a tissue section could easily approach millimolar concentrations, this is not an unreasonable possibility. We attempted to measure the absorbance within isolated cardiac myocytes as a function of excitation power in the TPEFM microscope by collecting all transmitted light. The two-photon absorbance was estimated from the fluorescence emission and increased as the square of the excitation light, as predicted. However, no significant change in total absorbance was observed with the increasing power and two-photon absorption as estimated from the emission. Thus, these initial studies suggest that the two-photon absorption within the focal plane is not significant, relative to the total tissue NIR absorbance under these conditions.

The secondary filter effect is the absorbance of the emitted light as it scatters through microns of tissues between the focal plane and the microscope objective. Thus, the secondary filter reflects the average optical properties of the tissue. Significant secondary emission filters have been demonstrated by a variety of investigators in UV one-photon excitation fluorescence studies with minimal tissue penetration (Chance and Schoener, 1962; Fralix et al., 1990; Koretsky et al., 1987; Leisey et al., 1994), including this study (Fig. 7). Thus, with the deeper penetration of TPEFM, it is not surprising that a significant secondary inner filter was observed (see Fig. 8). In the one-photon mode, with minimal tissue penetration, the liability of the secondary filters with oxygen tension in visible light was demonstrated (Fig. 7). The spectral characteristics and oxygen sensitivity were consistent with myoglobin and hemoglobin dominating the secondary tissue filters. As demonstrated in the ischemia time course, alterations in tissue myoglobin/hemoglobin absorption can significantly interfere with the absolute NAD(P)H emission amplitude resulting in numerous artifacts. For example, the initial decrease in NAD(P)H fluorescence observed with ischemia is primarily due to the deoxygenation of myoglobin and hemoglobin, not a change in [NAD(P)H], and the resting NAD(P)H signal in the steady-state ischemic state is also influenced by the optical properties of the tissue.

The contribution of the secondary inner filter in TPEFM was demonstrated by determining the spectral characteristics of NAD(P)H emission frequency as a function of the focal plane depth in the tissue. The NAD(P)H emission frequency red-shifted as the focal plane was advanced deeper into the tissue and the pathlength of the emitted light increased through the tissue. Thus, the inner filter is not only a function of the physiological state of the tissue (i.e., oxygenation) but also the depth at which the study is conducted. The red shift on the NAD(P)H emission was nearly identical to that found by Koretsky et al. with serial dilution of heart tissue (Koretsky et al., 1987) and is caused by the strong absorption of cytochromes, myoglobin, and hemoglobin in the ~420 nm region. This absorbance by myoglobin and hemoglobin is also present in the oxygenated state, with both oxygenated myoglobin/hemoglobin resulting in a NAD(P)H spectrum red-shifted from the true bound NAD(P)H emission spectrum. Because the secondary filter absorbance is a ''global'' measure of optical properties of the tissue, little information on the focal plane alone is encoded in the emission spectral characteristics. In the case of myoglobin, information on global tissue oxygenation could be inferred from the spectral shifts in NAD(P)H emission due to myoglobin absorbance (Leisey et al., 1994), but no information about the oxygenation at the imaging plane could be extracted. This apparent limitation is somewhat useful in characterizing the net tissue effects of physiological perturbations, but also has some advantages with regard to evaluating the heterogeneity of fluorescent signals in the focal plane. Because the tissue filter effects are global in nature they will uniformly affect the regional fluorescence emission within the focal plane. This implies that a difference in detected fluorescence emission within a focal plane cannot occur for a given probe due to changes in secondary tissue filtering characteristics. Thus, for some studies assessing regional heterogeneity within a focal plane, such as the different cellular compartments of mitochondria, the effects of tissue filters can be ignored. An exception to this might be situations directly under a large vein or artery where the absorption effects of hemoglobin might be regionally modulated.

Several approaches are available that can correct for secondary inner filter effects. The first is to collect emitted light only at the isobestic points of the oxygenated and deoxygenated myoglobin/hemoglobin absorbance spectra to minimize the effects from changes in tissue oxygenation on the emission amplitude (Brandes et al., 1994; Fralix et al., 1990; Koretsky et al., 1987). However, restricting the

collection of emitted light to the tissue isobestic points would greatly reduce the signal/noise ratio of the TPEFM experiment. This would also be the case if the entire spectrum of the sample was collected spectroscopically to correct for inner filter effects. Another correction scheme is the use of exogenously applied reference compounds to provide a correction for inner filter modifications (Koretsky et al., 1987). The use of an internal standard while monitoring NAD(P)H fluorescence may be a way of achieving a relative measure of NAD(P)H that is corrected not only for the internal filter, but also for the motion of the sample. Based on the spectra presented in Fig. 7, we propose that a probe with a stable emission in the 500–600 nm region that could be excited with 710–750 nm two-photon excitation, or simultaneously excited with another laser, would provide an adequate reference given the relatively fixed relationship between myoglobin and hemoglobin absorbance (500–600 and 400–480 nm, respectively). Several green fluorescence protein probes that could genetically be distributed throughout the tissue might be useful in this regard.

Motion

Attempting to collect image data on the order of several microns in vivo is difficult due to the naturally occurring tissue movement. Motion artifacts can decrease resolution or blur images in all three dimensions. Correction for these motion issues is best handled by immobilizing the tissue as effectively as possible, collecting the data as quickly as possible, and/or gating the acquisition to the motion using internal (i.e., the image itself) or external signals. Immobilization is a desirable solution because it will reduce the corrections required. However, in most tissues the pulsatile nature of the blood flow and respiratory activity will result in significant micron motions independent of the restraining scheme. This problem is compounded in muscle tissues where the motion of the tissue is the fundamental function of the tissue. One solution is to use NAD(P)H TPEFM to determine regional mitochondrial metabolic modifications associated with exercise at rest before and after skeletal muscle contraction. However, dynamic observations would be more desirable. Naturally, if the framing rate of the imaging experiment can be faster than the displacements occur, then the effects of motion can be minimized. The raster scanning of TPEFM results in an inherently slow imaging method that is susceptible to tissue motions when a ''large'' field of view of several hundred microns is being recorded. Rapid framing rates ($\sim$5 ms) can be obtained in TPEFM by reducing the field of view as far as a single line covering the area of interest and ''freezing'' muscle motion. Using this type of approach, dynamic measurements of sarcomere lengths, using the NAD(P)H signal from t-tubule localized mitochondria, may be possible during contraction cycles in vivo. However, for two-dimensional studies, current approaches are too slow for observations during a contraction cycle and a more rapid imaging strategy needs to be developed. The biggest obstacle will be to obtain adequate signal/noise without photodynamic damage. Like other imaging techniques, such as magnetic resonance imaging or computer-assisted tomography, gating data acquisitions to a particular position may be a partial solution. The gating signal for this approach could be from external sources (such as a muscle excitation pulse train) or using markers in the image itself. Potentially, a combination of these approaches might result in a feasible scheme for dynamic intracellular metabolic imaging during muscle contraction in vivo.

Skeletal muscle mitochondrial distribution

The functional significance of skeletal muscle cellular distribution of mitochondria has been difficult to assess in intact physiological systems. Although the highly ordered distribution of mitochondria is well appreciated, its cellular functional significance has mostly been speculated from ex vivo tissue static structural studies or within isolated cells (Jones, 1986; Kuznetsov et al., 1998). One interesting observation was the differential distribution of mitochondria in difference fiber types that permitted in vivo fiber typing similar to what has been done in vitro (Kuznetsov et al., 1998). Two general fiber types were resolved consistent with the slower (nominal IIA/D) and faster (IIB) fibers. The IIA/D contained high concentrations of more evenly distributed mitochondria with extensive paravascular mitochondria. A lower overall concentration of mitochondria was observed in IIB fiber types with the intersarcolemmal mitochondria almost exclusively located along either side of the t-tubule network, as confirmed by single-photon fluorescence and EM studies (Fig. 1). The localization of mitochondria to the t-tubule system may reflect several aspects of the structure/function relationship in the skeletal muscle. The t-tubule localization of mitochondria may simply be a mechanical consequence of optimizing contractile element cross-sectional area. This mechanically driven distribution of mitochondria is most obvious in the paranuclear mitochondria where they are in the ''eddies'' on opposite sides of the nucleus along the long axis of the cell where the fibers cannot interconnect to generate transcellular forces. The distribution of mitochondria may simply reflect the consequences of constructing muscle fibers in development (Forbes and Sperelakis, 1980). Therefore, the pattern of mitochondrial deposition might simply reflect the serial deposition of contractile elements in the muscle. Most intriguing is that the colocalization of t-tubules and mitochondria may represent a functional link. It has been suggested that the colocalization of mitochondria with the t-tubule/SR system may be related to local signaling by Ca^{2+} or even by ADP (Balaban, 2002; Kaasik et al., 2001; Ogata and Yamasaki, 1997). In addition, some muscarinic receptors have been localized along the t-tubules in heart muscle (Fu et al., 1994; Schulze et al., 1995), which suggests

that signaling between these sites and mitochondria might be facilitated by their colocalization.

Properly corrected for tissue inner filters, NAD(P)H TPEFM permits the dynamic evaluation of mitochondrial metabolic state in relation to its intracellular location in vivo. NAD(P)H TPEFM should permit the evaluation of several hypotheses concerning the role of mitochondria compartmentation in skeletal muscle cellular function. An obvious application for in vivo NAD(P)H TPEFM would be to study the role of perivascular mitochondria primarily located in the slower muscle fibers in regulating microvascular flow. In vivo NAD(P)H TPEFM, along with other TPEFM measurements of microvascular flow or oxygenation, would be helpful in evaluating the role of perivascular mitochondria in regulating or sensing microvascular flow. For example, the monitoring of these different cellular mitochondria populations during a simple ischemia/reperfusion series should be quite useful in delineating differential roles for the mitochondrial compartments in this physiological process.

We thank Dr. Zu-Xi Yu and the National Heart, Lung and Blood Institute's Pathology Core Facility for the electron and light microscopy and Mr. Michael Nauman for his aid in creating the mouse leg holder.

REFERENCES

Avi-Dor, Y., E. Lamdin, and N. O. Kaplan. 1963. Structural factors in the succinate-induced reduction of mitochondrial pyridine nucleotides. *J. Biol. Chem.* 238:2518–2528.

Balaban, R. S. 2002. Cardiac energy metabolism homeostasis: role of cytosolic calcium. *J. Mol. Cell. Cardiol.* 34:1259–1271.

Blinova, K., S. Carroll, S. Bose, A. V. Smirnov, J. J. Harvey, J. R. Knutson, and R. S. Balaban. 2004. The distribution of mitochondrial NADH fluorescence lifetimes: steady state kinetics of matrix NADH interactions. *Biochemistry.* In press.

Bose, S., S. French, F. J. Evans, F. Joubert, and R. S. Balaban. 2003. Metabolic network control of oxidative phosphorylation: multiple roles of inorganic phosphate. *J. Biol. Chem.* 278:39155–39165.

Brandes, R., V. M. Figueredo, S. A. Camacho, and M. W. Weiner. 1994. Compensation for changes in tissue light absorption in fluorometry of hypoxic perfused rat hearts. *Am. J. Physiol.* 266:H2554–H2567.

Brooke, M. H., and K. K. Kaiser. 1970. Muscle fiber types: how many and what kind? *Arch. Neurol.* 23:369–379.

Cahalan, M. D., I. Parker, S. H. Wei, and M. J. Miller. 2002. Two-photon tissue imaging: seeing the immune system in a fresh light. *Nature Rev. Immunol.* 2:872–880.

Carroll, S. L., M. G. Klein, and M. F. Schneider. 1995. Calcium transients in intact rat skeletal muscle fibers in agarose gel. *Am. J. Physiol.* 269: C28–C34.

Centonze, V. E., and J. G. White. 1998. Multiphoton excitation provides optical sections from deeper within scattering specimens than confocal imaging. *Biophys. J.* 75:2015–2024.

Chance, B., and H. Baltscheffsky. 1958. Respiratory enzymes in oxidative phosphorylation. VII. Binding of intramitochondrial reduced pyridine nucleotide. *J. Biol. Chem.* 233:736–739.

Chance, B., P. Cohen, F. Jobsis, and B. Schoener. 1962. Intracellular oxidation-reduction states in vivo. *Science.* 137:499–508.

Chance, B., and B. Schoener. 1962. Correlation of oxidation-reduction changes of intracellular reduced pyridine nucleotide and changes in electroencephalogram of the rat in anoxia. *Nauchni Tr. Vissh. Med. Inst. Sofiia.* 195:956–958.

Chance, B., and B. Thorell. 1959. Fluorescence measurements of mitochondrial pyridine nucleotide in aerobiosis and anaerobiosis. *Nature.* 184:931–934.

Chen, B. E., B. Lendvai, E. A. Nimchinsky, B. Burbach, K. Fox, and K. Svoboda. 2000. Imaging high-resolution structure of GFP-expressing neurons in neocortex in vivo. *Learn. Mem.* 7:433–441.

Chilibeck, P. D., D. G. Syrotuik, and G. J. Bell. 1999. The effect of strength training on estimates of mitochondrial density and distribution throughout muscle fibres. *Eur. J. Appl. Physiol.* 80:604–609.

Denk, W., K. R. Delaney, A. Gelperin, D. Kleinfeld, B. W. Strowbridge, D. W. Tank, and R. Yuste. 1994. Anatomical and functional imaging of neurons using 2-photon laser scanning microscopy. *J. Neurosci. Methods.* 54:151–162.

Denk, W., J. H. Strickler, and W. W. Webb. 1990. Two-photon laser scanning fluorescence microscopy. *Science.* 248:73–76.

Dunn, K. W., R. M. Sandoval, K. J. Kelly, P. C. Dagher, G. A. Tanner, S. J. Atkinson, R. L. Bacallao, and B. A. Molitoris. 2002. Functional studies of the kidney of living animals using multicolor two-photon microscopy. *Am. J. Physiol. Cell Physiol.* 283:C905–C916.

Eng, J., R. M. Lynch, and R. S. Balaban. 1989. Nicotinamide adenine dinucleotide fluorescence spectroscopy and imaging of isolated cardiac myocytes. *Biophys. J.* 55:621–630.

Estabrook, R. W. 1962. Fluorometric measurement of reduced pyridine nucleotide in cellular and subcellular particles. *Anal. Biochem.* 4:231–245.

Forbes, M. S., and N. Sperelakis. 1980. Structures located at the levels of the Z bands in mouse ventricular myocardial cells. *Tissue Cell.* 12:467–489.

Fralix, T. A., F. W. Heineman, and R. S. Balaban. 1990. Effects of tissue absorbance on NAD(P)H and Indo-1 fluorescence from perfused rabbit hearts. *FEBS Lett.* 262:287–292.

Fu, M., W. Schulze, W. P. Wolf, A. Hjalmarson, and J. Hoebeke. 1994. Immunocytochemical localization of M2 muscarinic receptors in rat ventricles with anti-peptide antibodies. *J. Histochem. Cytochem.* 42:337–343.

Hamalainen, N., and D. Pette. 1993. The histochemical profiles of fast fiber types IIB, IID, and IIA in skeletal muscles of mouse, rat, and rabbit. *J. Histochem. Cytochem.* 41:733–743.

Helmchen, F., K. Svoboda, W. Denk, and D. W. Tank. 1999. In vivo dendritic calcium dynamics in deep-layer cortical pyramidal neurons. *Nat. Neurosci.* 2:989–996.

Hoppeler, H., and M. Fluck. 2003. Plasticity of skeletal muscle mitochondria: structure and function. *Med. Sci. Sports Exerc.* 35:95–104.

Hoppeler, H., P. Luthi, H. Claassen, E. R. Weibel, and H. Howald. 1973. The ultrastructure of the normal human skeletal muscle. A morphometric analysis on untrained men, women and well-trained orienteers. *Pflugers Arch.* 344:217–232.

Huang, S., A. A. Heikal, and W. W. Webb. 2002. Two-photon fluorescence spectroscopy and microscopy of NAD(P)H and flavoprotein. *Biophys. J.* 82:2811–2825.

Jöbsis, P. D., C. A. Combs, and R. S. Balaban. 2004. Two-photon excitation fluorescence pH detection using 2, 3-dicyanohydroquinone: a spectral ratiometric approach. *J. Microsc.* In press.

Jones, D. P. 1986. Intracellular diffusion gradients of O2 and ATP. *Am. J. Physiol.* 250:C663–C675.

Kaasik, A., V. Veksler, E. Boehm, M. Novotova, A. Minajeva, and R. Ventura-Clapier. 2001. Energetic crosstalk between organelles: architectural integration of energy production and utilization. *Circ. Res.* 89:153–159.

Kasischke, K. A., H. D. Vishwasrao, P. J. Fisher, W. R. Zipfel, and W. W. Webb. 2004. Neural activity triggers neuronal oxidative metabolism followed by astrocytic glycolysis. *Science.* 305:99–103.

Kierdaszuk, B., H. Malak, I. Gryczynski, P. Callis, and J. R. Lakowicz. 1996. Fluorescence of reduced nicotinamides using one- and two-photon excitation. *Biophys. Chem.* 62:1–13.

Kleinfeld, D., P. P. Mitra, F. Helmchen, and W. Denk. 1998. Fluctuations and stimulus-induced changes in blood flow observed in individual capillaries in layers 2 through 4 of rat neocortex. *Proc. Natl. Acad. Sci. USA.* 95:15741–15746.

Konig, K., P. T. So, W. W. Mantulin, B. J. Tromberg, and E. Gratton. 1996. Two-photon excited lifetime imaging of autofluorescence in cells during UVA and NIR photostress. *J. Microsc.* 183:197–204.

Koretsky, A. P., L. A. Katz, and R. S. Balaban. 1987. Determination of pyridine nucleotide fluorescence from the perfused heart using an internal standard. *Am. J. Physiol.* 253:H856–H862.

Kuznetsov, A. V., O. Mayboroda, D. Kunz, K. Winkler, W. Schubert, and W. S. Kunz. 1998. Functional imaging of mitochondria in saponin-permeabilized mice muscle fibers. *J. Cell Biol.* 140:1091–1099.

Larson, D. R., W. R. Zipfel, R. M. Williams, S. W. Clark, M. P. Bruchez, F. W. Wise, and W. W. Webb. 2003. Water-soluble quantum dots for multiphoton fluorescence imaging in vivo. *Science.* 300:1434–1436.

Latimer, P., and E. Rabinowitch. 1959. Selective scattering of light by pigments in vivo. *Arch. Biochem. Biophys.* 84:428–441.

Leeson, C. R., and T. S. Leeson. 1969. Mitochondrial organization in skeletal muscle of the rat soft palate. *J. Anat.* 105:363–370.

Leisey, J. R., D. A. Scott, L. W. Grotyohann, and R. C. Scaduto, Jr. 1994. Quantitation of myoglobin saturation in the perfused heart using myoglobin as an optical inner filter. *Am. J. Physiol.* 267:H645–H653.

Levene, M. J., D. A. Dombeck, K. A. Kasischke, R. P. Molloy, and W. W. Webb. 2004. In vivo multiphoton microscopy of deep brain tissue. *J. Neurophysiol.* 91:1908–1912.

Masters, B. R., P. T. So, and E. Gratton. 1997. Multiphoton excitation fluorescence microscopy and spectroscopy of in vivo human skin. *Biophys. J.* 72:2405–2412.

Nuutinen, E. M. 1984. Subcellular origin of the surface fluorescence of reduced nicotinamide nucleotides in the isolated perfused rat heart. *Basic Res. Cardiol.* 79:49–58.

Ogata, T., and Y. Yamasaki. 1997. Ultra-high-resolution scanning electron microscopy of mitochondria and sarcoplasmic reticulum arrangement in human red, white, and intermediate muscle fibers. *Anat. Rec.* 248:214–223.

Piston, D. W., B. R. Masters, and W. W. Webb. 1995. Three-dimensionally resolved NAD(P)H cellular metabolic redox imaging of the in situ cornea with two-photon excitation laser scanning microscopy. *J. Microsc.* 178:20–27.

Raymackers, J. M., P. Gailly, M. C. Schoor, D. Pette, B. Schwaller, W. Hunziker, M. R. Celio, and J. M. Gillis. 2000. Tetanus relaxation of fast skeletal muscles of the mouse made parvalbumin deficient by gene inactivation. *J. Physiol.* 527:355–364.

Richmond, K. N., R. D. Shonat, R. M. Lynch, and P. C. Johnson. 1999. Critical PO(2) of skeletal muscle in vivo. *Am. J. Physiol.* 277:H1831–H1840.

Sartorius, C. A., B. D. Lu, L. Acakpo-Satchivi, R. P. Jacobsen, W. C. Byrnes, and L. A. Leinwand. 1998. Myosin heavy chains IIa and IId are functionally distinct in the mouse. *J. Cell Biol.* 141: 943–953.

Schulze, W., W. P. Wolf, M. L. Fu, R. Morwinski, I. B. Buchwalow, and L. Will-Shahab. 1995. Immunocytochemical studies of the Gi protein mediated muscarinic receptor-adenylyl cyclase system. *Mol. Cell. Biochem.* 147:161–168.

Sheik-Bahae, M., A. A. Said, T. H. Wei, D. J. Hagan, and E. W. Van Stryland. 1990. Sensitive measurement of optical nonlinearities using a single beam. *IEEE J. Quantum Electron.* 26:760–769.

Squirrell, J. M., D. L. Wokosin, J. G. White, and B. D. Bavister. 1999. Long-term two-photon fluorescence imaging of mammalian embryos without compromising viability. *Nat. Biotechnol.* 17:763–767.

Stenger, R. J., D. Spiro, R. E. Scully, and J. M. Shannon. 1962. Ultrastructural and physiologic alterations in ischemic skeletal muscle. *Am. J. Pathol.* 40:1–20.

Svoboda, K., W. Denk, D. Kleinfeld, and D. W. Tank. 1997. In vivo dendritic calcium dynamics in neocortical pyramidal neurons. *Nature.* 385:161–165.

Tamura, M., N. Oshino, B. Chance, and I. A. Silver. 1978. Optical measurements of intracellular oxygen concentration of rat heart in vitro. *Arch. Biochem. Biophys.* 191:8–22.

Totsuka, Y., Y. Nagao, T. Horii, H. Yonekawa, H. Imai, H. Hatta, Y. Izaike, T. Tokunaga, and Y. Atomi. 2003. Physical performance and soleus muscle fiber composition in wild-derived and laboratory inbred mouse strains. *J. Appl. Physiol.* 95:720–727.

Wilson, B. C., M. S. Patterson, S. T. Flock, and J. D. Moulton. 1989. The optical absorption and scattering properties of tissues in the visible and near-infrared wavelength range. *In* Light in Biology and Medicine. R. H. Douglas, J. Moan, F. Dall'Acqua, editors. Plenum Press, New York, NY and London, UK.

Zipfel, W. R., R. M. Williams, R. Christie, A. Y. Nikitin, B. T. Hyman, and W. W. Webb. 2003. Live tissue intrinsic emission microscopy using multiphoton-excited native fluorescence and second harmonic generation. *Proc. Natl. Acad. Sci. USA.* 100:7075–7080.